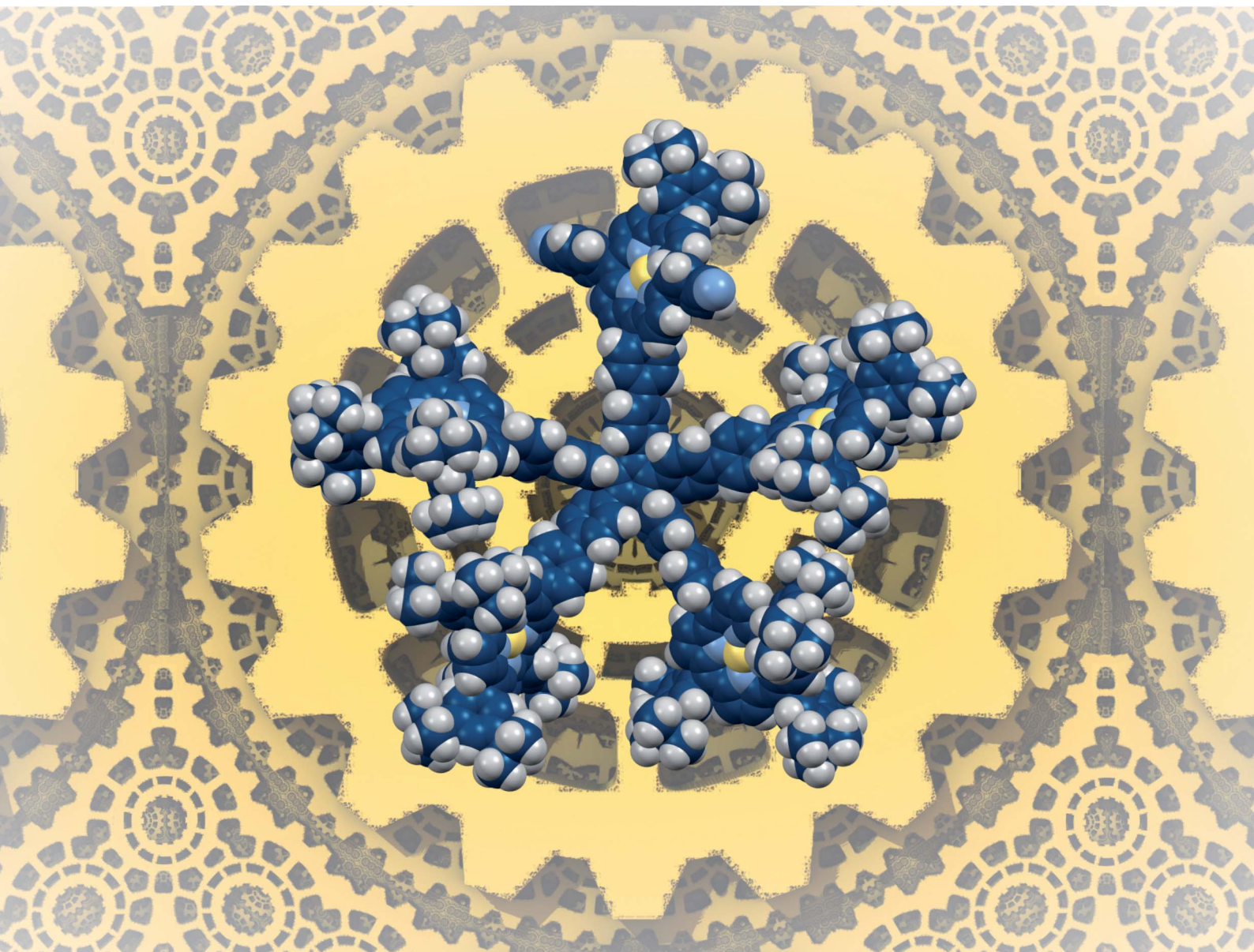


# Chemical Science

[rsc.li/chemical-science](https://rsc.li/chemical-science)



ISSN 2041-6539

## EDGE ARTICLE

Claire Kammerer, Gwénaël Rapenne *et al.*  
Desymmetrised pentaporphyrinic gears mounted on  
metallo-organic anchors

## EDGE ARTICLE

[View Article Online](#)  
[View Journal](#) | [View Issue](#)



Cite this: *Chem. Sci.*, 2021, **12**, 4709

All publication charges for this article have been paid for by the Royal Society of Chemistry

## Desymmetrised pentaporphyrinic gears mounted on metalloc-organic anchors†

Seifallah Abid, <sup>a</sup> Yohan Gisbert, <sup>a</sup> Mitsuru Kojima, <sup>b</sup> Nathalie Saffon-Merceron, <sup>c</sup> Jérôme Cuny, <sup>d</sup> Claire Kammerer <sup>\*a</sup> and Gwénaël Rapenne <sup>\*ab</sup>

Mastering intermolecular gearing is crucial for the emergence of complex functional nanoscale machineries. However, achieving correlated motion within trains of molecular gears remains highly challenging, due to the multiple degrees of freedom of each cogwheel. In this context, we designed and synthesised a series of star-shaped organometallic molecular gears incorporating a hydrotris(indazolyl) borate anchor to prevent diffusion on the surface, a central ruthenium atom as a fixed rotation axis, and an azimuthal pentaporphyrinic cyclopentadienyl cogwheel specifically labelled to monitor its motion by non-time-resolved Scanning Tunneling Microscopy (STM). Desymmetrisation of the cogwheels was first achieved sterically, *i.e.* by introducing one tooth longer than the other four. For optimal mechanical interactions, chemical labelling was also investigated as a preferential way to induce local contrast in STM images, and the electronic properties of one single paddle were modulated by varying the porphyrinic scaffold or the nature of the central metal. To reach such a structural diversity, our modular synthetic approach relied on sequential cross-coupling reactions on a penta(*p*-halogenophenyl) cyclopentadienyl ruthenium(*II*) key building block, bearing a single pre-activated *p*-iodophenyl group. Chemoselective Sonogashira or more challenging Suzuki–Miyaura reactions allowed the controlled introduction of the tagged porphyrinic tooth, and the subsequent four-fold cross-couplings yielded the prototypes of pentaporphyrinic molecular gears for on-surface studies, incorporating desymmetrised cogwheels over 5 nm in diameter.

Received 20th November 2020

Accepted 13th February 2021

DOI: 10.1039/d0sc06379g

[rsc.li/chemical-science](http://rsc.li/chemical-science)

## 1. Introduction

Prompted by the pioneering studies of Sauvage, Stoddart and Feringa,<sup>1</sup> the field of artificial molecular machines has witnessed an impressive development over the last decades and different types of machines have been reported,<sup>2</sup> some of them being technomimetic<sup>3</sup> such as syringes,<sup>4</sup> wheelbarrows,<sup>5</sup> vehicles,<sup>6</sup> scissors,<sup>7</sup> and elevators.<sup>8</sup> In addition, control over directionality of motion gave rise to artificial rotary motors<sup>9</sup> responding to chemical,<sup>10</sup> light,<sup>11</sup> or electric stimuli.<sup>12</sup> A vast majority of these machines have been studied collectively in solution or at interfaces, leading to average behaviour over populations of molecules. However, with the advent of scanning

probe microscopy, resolution down to the atomic scale has been reached, thus allowing for in-depth investigations into nanoscale mechanics on single molecules adsorbed on surfaces.<sup>13</sup> Even a race of nanocars was proposed<sup>14</sup> and organised in 2017,<sup>15</sup> showing that these nanomachines are now studied at the single-molecule level by many research teams worldwide.

With this large array of artificial molecular machines at hand, the next step is now to master the assembly of several of such individual modules into complex functional nanoscale machineries. In this regard, gear systems appear as essential elementary units allowing the mechanical transmission of information over (long) distances and the conversion of the motive power of a motor through synchronised disrotatory motion of the cogwheels. Ancient machineries such as the Antikythera mechanism, which dates back to the Hellenistic period (150–100 BC), already incorporated decimeter-scale gear components in their structure.<sup>16</sup> Over the centuries, miniaturisation of solid state cogwheels has been pushed forward as a function of available technology, with the smallest reported cogwheels having a diameter of 70 nm, obtained by e-beam lithography.<sup>17</sup>

As opposed to this top-down approach that is close to reaching its physical limits in terms of object size, molecular gear systems have alternatively been obtained by

<sup>a</sup>CEMES, Université de Toulouse, CNRS, 29 Rue Marvig, F-31055 Toulouse Cedex 4, France. E-mail: rapenne@cemes.fr

<sup>b</sup>Division of Materials Science, Nara Institute of Science and Technology, NAIST, 8916-5 Takayama-cho, Ikoma, Nara 630-0192, Japan

<sup>c</sup>Université de Toulouse, UPS, Institut de Chimie de Toulouse, ICT FR 2599, 118 Route de Narbonne, 31062 Toulouse, France

<sup>d</sup>LCPQ, Université de Toulouse, CNRS, 118 Route de Narbonne, F-31062 Toulouse Cedex 9, France

† Electronic supplementary information (ESI) available. CCDC 2039772 and 2039773. For ESI and crystallographic data in CIF or other electronic format see DOI: 10.1039/d0sc06379g



a monumentalisation strategy *via* the controlled assembly of specifically designed molecular cogwheels. In this regard, the  $C_3$ -symmetric triptycene fragment has been extensively investigated as a three-blade cogwheel archetype in intramolecular gearing systems studied in solution. Pioneering examples of covalent bis-triptyceny structures with intersecting rotation axes (*i.e.* bevel gear prototypes, Fig. 1a) were independently reported in 1980 by Mislow<sup>18</sup> and Iwamura,<sup>19</sup> who unambiguously demonstrated the disrotatory correlated motion of the meshed cogwheels by inserting a tag on one blade of each cogwheel.

Analogous bis-triptyceny systems bearing different linkers were reported over the years,<sup>24</sup> some of which exhibited very elegant switch function in response to a chemical<sup>25</sup> or photochemical<sup>26</sup> stimulus. In a similar approach, prototypes of spur gears, involving parallel rotation axes, were developed more recently (Fig. 1b) and the impact of the inter-triptycene distance on the gearing fidelity (*i.e.* proportion of geared rotations over gear slippage) was highlighted.<sup>21,27</sup> The complexity of intramolecular gearing systems has been further enhanced by varying the nature of the cogwheels<sup>28</sup> or by multiplying the number of meshed cogwheels.<sup>29</sup> However, in all these systems designed for *in-solution* studies, gearing mechanisms are inherently limited to intramolecular correlated motion of sub-molecular fragments bound to a rigid scaffold, which is required to maintain the distance and relative orientation of the rotation axes. To achieve intermolecular gearing and thus allow correlated motion over longer distances, pre-organisation of the assembly of cogwheels is required (Fig. 2), with (i) a linear arrangement leading to a train of gears, (ii) a parallel orientation of the rotation axes (depicted in red), and (iii) appropriate and locked intermolecular distances leading to proper intertwining of the teeth.

With this aim in view, specifically designed molecular cogwheels have been investigated as solid state self-

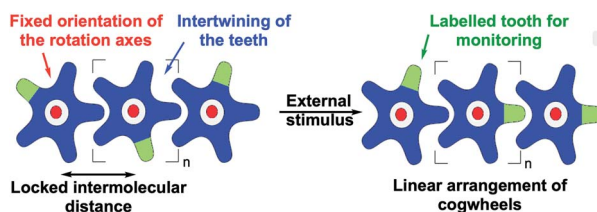


Fig. 2 Schematic representation of the key parameters to be considered in the design of trains of molecular gears to achieve intermolecular correlated rotation in response to an external stimulus: top views of a train of hypothetical star-shaped cogwheels (in blue) incorporating a labelled tooth (in green) and mounted on rotation axes (in red) at fixed intermolecular distances, before and after an external stimulus leading to correlated motion.

assemblies,<sup>30</sup> or alternatively deposited on surfaces and studied at the single molecule scale by means of Scanning Tunneling Microscopy (STM).<sup>31</sup> To date, the smallest known functional train of gears deposited on a surface has been constructed on Au(111) using star-shaped pentaarylcyclopentadienyl derivatives as cogwheels, taking advantage of their radical state to promote chemical anchoring on the metallic surface (Fig. 1c).<sup>22</sup> This anchoring locks the inter-cogwheel distance and favours intermolecular correlated motion over diffusion of the neighbouring species. Under these conditions, rotation of the driver cogwheel, induced by mechanical manipulation using the STM tip, was, for the first time, successfully propagated to two further molecules. The disrotatory correlated motion of these three cogwheels was evidenced by comparison of STM images, exploiting the presence of one *tert*-butyl substituent per molecule as a steric tag. As an alternative to chemical anchoring to fix the multimolecular gearing system, single metallic atoms have been deposited on a Pb(111) surface and hexaarylbenzene-based cogwheels (Fig. 1d) have been successfully mounted on top of such ad-atoms thus acting as the rotation axis.<sup>23,32</sup> These approaches, which gave rise to the first functional trains of molecular gears on a surface, fulfill several of the criteria detailed in Fig. 2. However, they rely on the *in situ* generation of the rotation axes after the deposition of the molecular cogwheels on the surface.

As an alternative, it also appears possible to incorporate a metallic rotation axis in a molecular structure prior to deposition by means of coordination chemistry, and bring the pre-assembled functional metallo-organic species on the surface. This approach was exploited in the design, synthesis and on-surface study of a family of ruthenium-based rotary molecular machines,<sup>33</sup> and in particular of an electron-fueled molecular motor.<sup>12b</sup> The central ruthenium atom acts as a ball bearing between an azimuthal pentaarylcyclopentadienyl rotating subunit and a hydrotris(indazolyl)borate stator, specifically functionalised with thioether groups. This scorpionate ligand lifts away from the surface the ruthenium rotation axis and thus the rotor, while affording tight anchoring on noble metal surfaces at low temperature.<sup>34</sup> It is important to note here that translation of such complexes by STM lateral manipulation is still possible at 77 K while diffusion is totally frozen at 4 K,

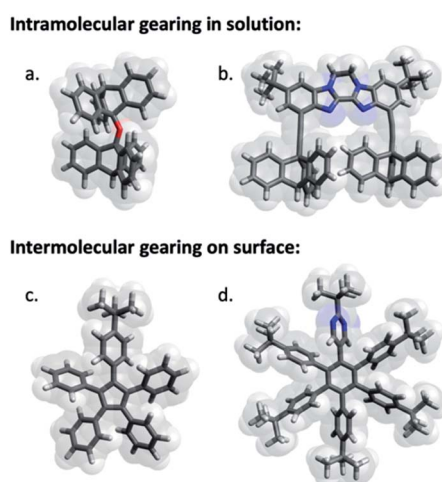


Fig. 1 Selection of pioneering examples of molecular cogwheel systems exhibiting intramolecular gearing in solution (a and b) or intermolecular gearing when anchored on a surface (c and d). These selected examples have been reported by (a) Iwamura,<sup>20</sup> (b) Siegel,<sup>21</sup> (c) Moresco<sup>22</sup> and (d) Soe.<sup>23</sup>



which allows a dedicated spatial molecular arrangement to be set up by STM manipulation and subsequently frozen. This ruthenium-based scaffold seemed particularly well adapted for the construction of trains of molecular gears on surfaces, with control over the rotation axis orientation, the intermolecular distance and the height of the cogwheels, decoupled from the surface. The cyclopentadienyl core was thus functionalised to mimic star-shaped cogwheels, with teeth ranging from pseudo-monodimensional biaryl fragments to bidimensional porphyrinic paddles for an optimal intermolecular transmission of motion.<sup>35</sup> The resulting family of prototypes incorporate rotor subunits with a  $C_5$  symmetry (*i.e.* carrying five identical teeth), which will prevent direct monitoring of motions on a surface based on static STM images.

In order to get a deeper understanding of the single-molecule mechanics of such ruthenium-based cogwheel prototypes, it appears crucial for on-surface studies to lower the symmetry of the upper rotating subunit. This may be achieved by varying the shape of one of the five teeth (*i.e.* introducing a steric tag) or by chemically inducing a change in the STM contrast of one of the teeth (*i.e.* introducing a chemical tag). This labelling strategy is commonly applied to monitor molecular motions by STM, on the single molecule scale or within self-assemblies, and discrimination is usually performed by adding or removing a bulky group (steric tag)<sup>12b,22</sup> or by inserting nitrogen atoms in the molecular backbone (chemical tag).<sup>31</sup>

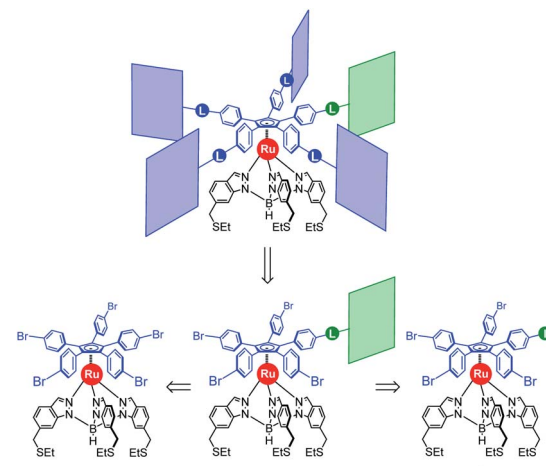
The desymmetrisation of extended ruthenium-based porphyrinic cogwheels was thus tackled, exploiting the length of the paddles and the electronic features of the porphyrins as steric and chemical tags, respectively. Herein, we report the design supported by DFT calculations, the modular synthesis and the characterisation of a series of desymmetrised cogwheel prototypes bearing one labelled porphyrinic paddle.

## 2. Results and discussion

Lowering the symmetry of the star-shaped ruthenium-based cogwheels while maintaining their structural diversity implies the development of a modular synthetic approach, allowing for a controlled introduction of a sterically- or chemically-tagged porphyrinic tooth.

### 2.1. Synthetic strategies towards desymmetrised pentaporphyrinic cyclopentadienyl cogwheels

Our general strategy for the synthesis of ruthenium-based rotary machines relies on a post-functionalisation of a piano-stool ruthenium complex as the key intermediate, incorporating the thioether-functionalised hydrotris(indazolyl)borate tripod in combination with a pentaaryl-cyclopentadienyl ligand. In anticipation of post-functionalisation *via* multiple transition metal-catalysed cross-coupling reactions, the cyclopentadienyl rotor part is pre-activated and thus it carries five *p*-halogenophenyl groups. Starting from the corresponding pentabrominated<sup>36</sup> or pentaiodinated<sup>35</sup> precursor, five-fold cross-coupling reactions gave rise to a variety of cogwheel prototypes of increasing diameter, with five identical teeth such as 4,4'-biphenyl fragments,



**Scheme 1** Retrosynthetic approaches towards desymmetrised cyclopentadienyl cogwheels, via statistical (left) vs. chemoselective (right) routes (L = linker).

carbazoles, BODIPYs and porphyrins. It is, however, important to mention here that the reactivity of the bromophenyl groups in the key precursor is dramatically reduced by the proximity of the electron-rich cyclopentadienyl platform, compared to bromobenzene as the reference, thus requiring highly active catalysts for such transformations. It has also been observed that the five halogenated positions react independently. A purely statistical approach for the desymmetrisation of the cyclopentadienyl cogwheel, with a concomitant introduction of both coupling partners in a 4 to 1 ratio, is thus doomed to failure and controlled synthetic routes were devised.

From a retrosynthetic point of view, desymmetrised cyclopentadienyl cogwheels with one discriminated tooth may stem from a synthetic intermediate carrying this distinct tooth, along with four halogenophenyl moieties still available for a final four-fold cross-coupling (Scheme 1). The mono-functionalised intermediate may in turn be obtained according to two distinct strategies, relying on statistical (Scheme 1, bottom left) *vs.* chemoselective (bottom right) approaches. The statistical strategy leads back to the symmetrical penta(*p*-bromophenyl)-appended precursor 2, and implies the introduction of the distinct tooth *via* a Suzuki–Miyaura or Sonogashira cross-coupling under statistical conditions, presumably with moderate efficiency due to the formation of various by-products. As an alternative, a selective pathway has been envisioned, relying on the discrimination of aryl halides in cross-coupling reactions leading to ethynylaryl<sup>37</sup> or biaryl<sup>38</sup> patterns. A universal unsymmetrical 1,2,3,4,5-penta(*p*-halogenophenyl)cyclopentadienyl ruthenium(II) precursor with a single pre-activated *p*-iodophenyl group (**1**) was thus designed and synthesised,<sup>39</sup> to allow for a chemoselective mono-functionalisation as a starting point for the synthesis of pentaporphyrinic cogwheels incorporating one sterically- or chemically-tagged tooth.

### 2.2. Steric desymmetrisation

As opposed to translation motion, the STM characterisation of rotary motion of  $C_n$ -symmetric objects on surfaces is not



straightforward due to the absence of time resolution. This issue is commonly overcome by sterically lowering the symmetry of the objects, thus allowing the motion to be monitored by comparing static images recorded before and after the stimulus. This strategy was in particular applied to star-shaped cyclopentadienyl derivatives, bearing one truncated tolyl arm among ferrocenylphenyl arms<sup>12b</sup> or one extended *p*-*tert*-butylphenyl tooth compared to the remaining phenyl teeth.<sup>22</sup> In the case of ruthenium-based cogwheels, the length of the linker between the cyclopentadienyl core and the tetrapyrrole macrocycle was chosen as the key parameter for steric labelling, while keeping the structure of the porphyrin constant. Indeed, in our previous work towards symmetric cogwheels,<sup>35</sup> the diameter of the rotating platform could be successfully modulated by changing the structure of the linker. While a five-fold Suzuki–Miyaura coupling applied to the symmetrical pentabrominated precursor **2** delivered 4,4'-biphenyl patterns, a five-fold Sonogashira reaction afforded phenylethynylphenyl spacers leading to a cogwheel diameter up to 5 nm. Interestingly, the Sonogashira coupling was successfully carried out under very mild conditions (45 °C, 24 h, in triethylamine) starting from the symmetrical pentaiodinated precursor, while the standard pentabrominated counterpart **2** required much harsher conditions (95 °C, 48 h, in DMF/diisopropylamine). This dramatic change was expected in view of the higher reactivity of aryl iodides than that of aryl bromides in Sonogashira reactions,<sup>37</sup> but most importantly it opens the way for chemoselective monofunctionalisation of the unsymmetrical mono-iodinated key precursor **1**. This will thus be exploited to produce sterically tagged cogwheels, incorporating one tooth longer than the other four, while keeping the structure of the external porphyrins constant. According to our strategy, a chemoselective Sonogashira coupling reaction on the pre-activated precursor **1** will provide a monofunctionalised intermediate with a single long porphyrinic tooth, and the four remaining *p*-bromophenyl moieties will then undergo a four-fold Suzuki–Miyaura coupling to introduce shorter biphenyl-based teeth.

For the series of ruthenium-based cogwheels, nickel(II) porphyrins have been selected as rigid and flat paddles, in view of the high stability of the nickel centre which avoids any metal exchange during studies on metallic surfaces. Such A<sub>3</sub>B-type macrocycles carry 3,5-di-*tert*-butylphenyl substituents on three *meso* positions which increase solubility during in-solution synthesis and limit π–π stacking on the surface among neighbouring cogwheels, which may hamper transmission of motion. The fourth *meso* position is functionalised in anticipation of Sonogashira and Suzuki–Miyaura reactions with a phenylethynyl group (**3**) or a phenylboronic acid pinacol ester moiety (**4**), respectively (Fig. 3). A<sub>3</sub>B-type porphyrins **3** and **4** were synthesised under Lindsey statistical conditions starting from pyrrole and appropriate benzaldehyde derivatives, and metalation was next performed in the presence of nickel(II) acetylacetone (see the ESI section†). With both porphyrinic coupling partners in hand, the synthesis of sterically tagged cogwheel **9** via a selective approach was tackled (Scheme 2). The higher reactivity of aryl iodides than that of their bromide counterparts in Sonogashira couplings was exploited for the

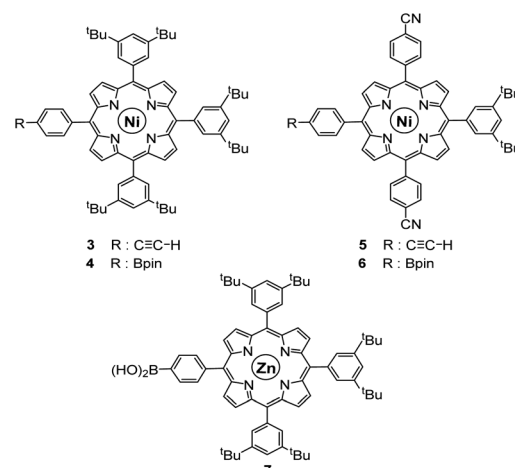


Fig. 3 Structure of porphyrins **3–7** used as coupling partners in the synthesis of desymmetrised cogwheel prototypes.

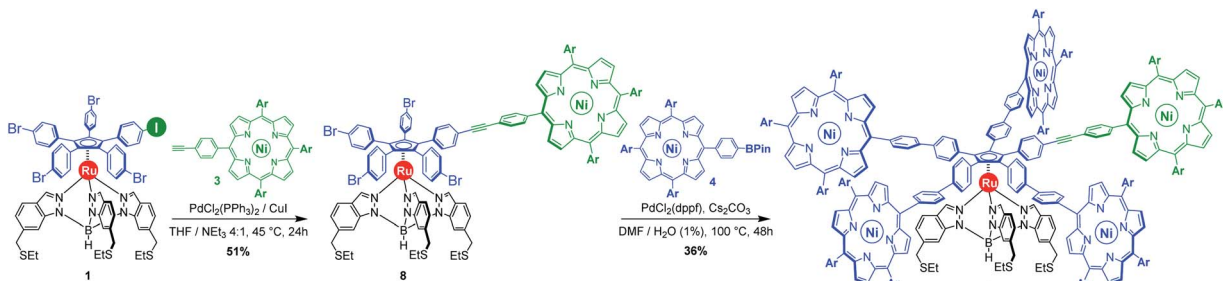
monofunctionalisation of key precursor **1**. The latter reacted under mild conditions with 5-(ethynylphenyl)porphyrin **3** in the presence of PdCl<sub>2</sub>(PPh<sub>3</sub>)<sub>2</sub> and CuI as cocatalysts to afford the expected monoporphyrinic complex **8** in 51% yield. The four remaining *p*-bromophenylene groups were subsequently submitted to Suzuki–Miyaura coupling conditions in the presence of an excess of porphyrin **4** to give the pentaporphyrinic complex **9** in 36% yield. The structure of this sterically tagged cogwheel prototype incorporating five identical porphyrinic paddles but one longer linker was confirmed by combined characterisation techniques, unambiguously showing the presence of four 4,4'-biphenyl patterns and a single phenylethynylphenyl moiety acting as a steric tag.

Incorporation of a steric tag in molecular scaffolds is a standard method to evidence rotary motion in STM studies. However, in gearing systems this structural variation might modify the interlocking of teeth and thus intermolecular interactions, which may prevent the correlated motion of neighbouring cogwheels.<sup>22</sup> As an alternative, we envisioned to induce a change in the STM contrast of one single tooth while keeping the shape of all cogwheels identical.

### 2.3. Chemical desymmetrisation

Contrast in STM images is correlated to local variations of tunneling current intensity at given tip height and bias voltage when scanning the surface. Submolecular contrast thus depends on the distribution of electronic density within a molecular object adsorbed on a surface. Such a submolecular contrast is routinely exploited to evidence the rotary motion of highly symmetric molecules, as in the case of the synchronised rotation of double-decker self-assemblies unambiguously evidenced thanks to the dipolar character of the upper porphyrinic deck.<sup>40</sup> Chemical desymmetrisation has also been performed by intentionally substituting one submolecular fragment with an isosteric group featuring distinct electronic properties. By way of example, the hexaarylbenzene cogwheel used in the first example of intermolecular gearing on the surface<sup>31a</sup>





**Scheme 2** Synthesis of the sterically tagged cogwheel 9, incorporating one longer tooth (in green), via sequential chemoselective Sonogashira and four-fold Suzuki–Miyaura cross-coupling reactions. Ar = 3,5-di-*tert*-butylphenyl.

incorporates five *tert*-butylphenyl teeth and a single *tert*-butylpyrimidyl fragment as the N-tagged tooth, inducing a contrast on a Cu(111) surface.

For the ruthenium-based molecular gears, an optimal design favouring interlocking and gearing motion relies on cogwheels bearing teeth of identical length and with homogeneous peripheral shapes for the paddles. We thus aim at a chemical desymmetrisation involving a variation of the electronic properties of a single porphyrin, while keeping an identical substitution pattern at the 5,15 positions. In the present case, a bright contrast located on the tagged paddle will be obtained in STM images if the LUMO is centred on this discriminated porphyrin.

**2.3.1. Design of the discriminated paddle and DFT calculations.** Electronic properties of metallated porphyrins can be modulated by changing the nature of the substituents carried by the tetrapyrrole core or by changing the nature of the central metal. Taking nickel(II) porphyrins carrying three 3,5-di-*tert*-butylphenyl *meso* substituents as reference paddles, it was first envisioned to introduce electron-withdrawing groups such as 4-cyanophenyl moieties on the 10, 20 positions of the tagged macrocycle, and DFT calculations were undertaken to probe the structural and electronic features of the corresponding desymmetrised cogwheel prototypes. DFT calculations were performed in a vacuum using Gaussian 09 software,<sup>41a</sup> using the

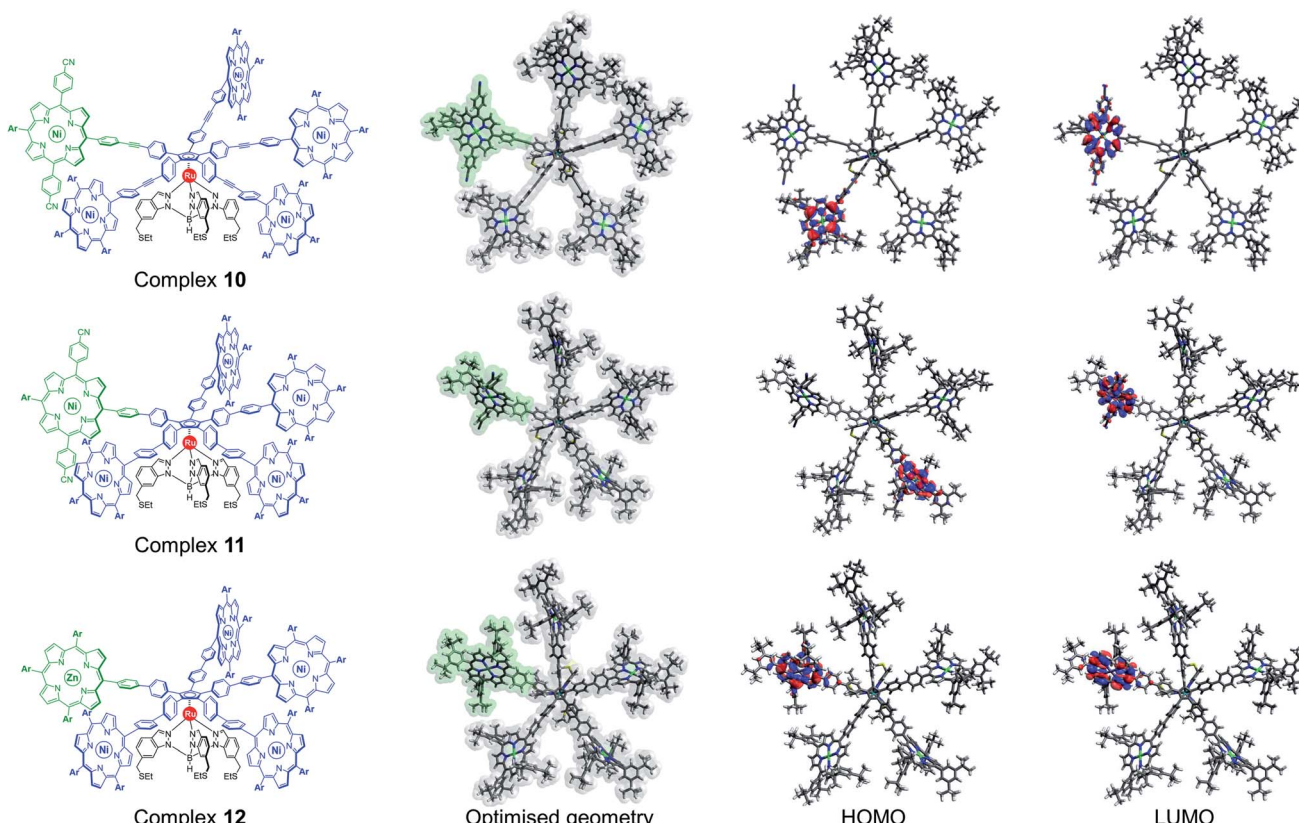


**Fig. 4** Chemical structure, DFT-optimised geometry (with the distinct porphyrin unit highlighted in green) and HOMO–LUMO maps of desymmetrised pentaporphyrinic ruthenium complexes 10, 11 and 12 (Ar = 3,5-di-*tert*-butylphenyl).

B3LYP functional, the 6-31G(d,p) all-electron basis set for light elements and the LANL2DZ basis set combined with effective core potentials for metallic centers. The geometries of complexes **10** and **11**, incorporating longer phenylethynylphenyl and shorter biphenyl spacers, respectively, were first optimised (Fig. 4, top and middle rows). Interestingly, they revealed that, in the gas phase, the nature of the linker has an impact on the arrangement of peripheral porphyrins. With the longer phenylethynylphenyl fragment (complex **10**), the five porphyrins are very slightly tilted compared to the central cyclopentadienyl core, which is not optimal for an efficient intertwining of neighbouring paddles. On the other hand, the biphenylene pattern (complex **11**) induces more steric constraint and leads to higher tilt angles of the porphyrins. Cogwheels incorporating 4,4'-biphenyl linkers thus appear more suitable for possible gearing motion due to more restricted degrees of freedom of the paddles.

In order to assess the possibility of forming a train of gears with this cogwheel design, further calculations were performed using the GFN2-xTB semi-empirical tight-binding model<sup>41b</sup> specifically dedicated to describe organometallic compounds containing a few thousand atoms. It also includes an accurate description of noncovalent interactions as required in the present study. The geometry of two interacting cogwheels **11** was optimised for three different distances between the rotation axes (Ru-Ru distances): 35.3, 37.5 and 41.2 Å. The final optimised structures are presented in Fig. S12–S14 in the ESI section.† According to these structures, even with the smallest distance (35.3 Å), the space between two porphyrinic paddles is sufficient to accommodate a paddle from the neighbouring cogwheel, thus demonstrating that this architecture leads to a proper intertwining of the teeth, which is a prerequisite for correlated rotation.

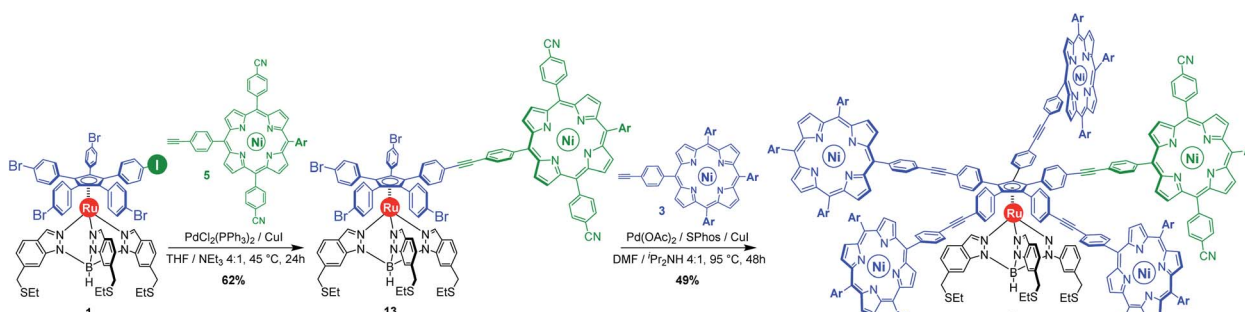
However, these results obtained in the gas phase have to be confirmed by further calculations considering the molecule adsorbed *via* its thioether-functionalised tripod on a metallic surface. Even if the cyclopentadienyl platform carrying the five porphyrins is lifted up and thus strongly decoupled from the surface, important changes in paddle conformations might result from interactions between porphyrinic *meso* 10,20-substituents and the metallic surface, especially in the case of 4-cyanophenyl moieties inserted on the tagged paddle. Moreover,

it has been shown that the tripodal ligand undergoes a twist of the indazole fragments when adsorbed on a metal surface, leading to helical chirality of the hydrotris(indazolyl)borate subunit as a 1 : 1 ratio of right- and left-handed propellers.<sup>12b</sup> Owing to important steric interactions, tilting of the indazoles is expected to affect the orientation of the phenyl moieties directly connected to the cyclopentadienyl ring<sup>13e</sup> which may thus induce helical chirality on the rotating cogwheel. In such a case, it could be envisioned to build trains of gears with alternating right- and left-handed cogwheels to allow propagation of disrotatory motion.

From an electronic point of view, regardless of the nature of the linker, the frontier orbitals of desymmetrised ruthenium complexes **10** and **11** are centred exclusively on the porphyrinic units (Fig. 4). As expected from the incorporation of electron-withdrawing substituents, the LUMO is located on the discriminated porphyrin carrying the 4-cyanophenyl substituents, which is promising to obtain a bright contrast on this paddle in STM studies.

Alternatively, the electronic properties of porphyrins can also be modulated by the presence or not of a coordinated metal, and by its nature. In the case of molecular gears to be actuated on a metallic surface, it appears highly desirable to use metal porphyrins as paddles since such free-base macrocycles are known to undergo metal insertion on noble metal surfaces.<sup>42</sup> In addition, having a single free-base porphyrin as a discriminated paddle may lead to intermolecular scrambling in solution, which might in fine produce anisotropic population of cogwheel prototypes. DFT calculations were thus undertaken to probe the electronic features of a cogwheel prototype carrying five identical A<sub>3</sub>B-type tetrapyrrolic scaffolds, with four nickel(II) and one distinct zinc(II) metallic centres. The optimised geometry of the star-shaped complex **12** involving 4,4'-biphenyl linkers around the cyclopentadienyl core and the corresponding frontier orbitals are presented in Fig. 4 (bottom row). Interestingly, both the HOMO and LUMO orbitals are centred on the distinct zinc(II) porphyrin, which is again likely to produce contrast in STM images.

This preliminary study based on DFT calculations highlighted two promising ways of inducing a chemical desymmetrisation of pentaporphyrinic cogwheel prototypes, while



**Scheme 3** Synthesis of the chemically-tagged cogwheel **10**, incorporating one distinct electron-deficient porphyrinic macrocycle (in green), via sequential Sonogashira cross-coupling reactions. Ar = 3,5-di-*tert*-butylphenyl.



keeping their shape unchanged. The synthesis of the three candidates was then tackled.

**2.3.2. A distinct porphyrinic scaffold as a chemical tag.** The preparation of chemically-tagged cogwheel **10** with phenylethynylphenyl spacers was first addressed in view of the high chemoselectivity achieved for the Sonogashira cross-coupling of monoiodinated precursor **1** (*vide supra*). Our strategy thus relied on sequential one- and four-fold Sonogashira couplings (Scheme 3). According to our design, nickel(II) A<sub>3</sub>B-type porphyrin **3** and nickel(II) *trans* A<sub>2</sub>BC-type porphyrin **5**, incorporating 4-cyanophenyl groups on the 10- and 20-*meso* positions and an ethynylphenyl moiety on the 5-position (Fig. 3), were targeted as coupling partners and subsequently synthesised (see the ESI section†).

With those two distinct nickel(II) porphyrinic macrocycles as coupling partners, the synthesis of cogwheels incorporating one chemically-discriminated porphyrin paddle was tackled. Single functionalisation of the mono(*p*-iodophenyl) key precursor **1** was carried out with 2 equiv. of *trans* A<sub>2</sub>BC porphyrin **5** (Scheme 3). The reaction occurred at 45 °C in the presence of PdCl<sub>2</sub>(PPh<sub>3</sub>)<sub>2</sub> (10 mol%) and CuI (6 mol%) as a catalytic system in a mixture of tetrahydrofuran and triethylamine (4 : 1). At this temperature, almost no side product resulting from the competitive oxidative addition of bromophenyl moieties was observed. After 24 h, ruthenium complex **13** bearing a single porphyrin as a result of the chemoselective Sonogashira coupling was isolated in 62% yield as a red solid.

Single crystals suitable for X-ray diffraction were successfully obtained by slow evaporation of a solution of **13** in a mixture of benzene and methanol (Fig. 5). The structure confirms the presence of the phenylethynylphenyl pattern as a linker between the cyclopentadienyl and porphyrin cores, with a torsion angle of 20° between both phenylene units. In the

solid state, it appears that the tetrapyrrole macrocycle lies almost parallel to the central cyclopentadienyl ring, with a distance of 2.6 nm between the centre of the Cp ring and the outer *tert*-butyl carbons located on the porphyrin *trans* *meso* substituent. The structure also confirms the presence of four remaining *p*-bromophenyl moieties available for further cross-couplings.

Insertion of four identical porphyrinic paddles was next attempted with A<sub>3</sub>B-type ethynylphenylporphyrin **3** (6 equiv., *i.e.* 1.5 equiv./Br) as the coupling partner. After optimisation of the reaction conditions, it appeared that the Buchwald catalyst showed high efficiency in promoting the Sonogashira coupling of the very poorly reactive bromophenylenes. Using a combination of Pd(OAc)<sub>2</sub> (40 mol%, *i.e.* 10 mol%/Br) and SPhos ligand (80 mol%) as the precatalyst, with CuI (30 mol%) as the second catalyst, the desired unsymmetrical pentaporphyrinic cogwheel **10** was isolated in 49% yield after 48 h at 95 °C in a DMF/diisopropylamine (4 : 1) mixture. This first example of a chemically-tagged ruthenium-based cogwheel was fully characterised (*vide infra*), thereby unambiguously confirming the presence of the five identical phenylethynylphenyl spacers carrying distinct porphyrinic units.

Next, the synthesis of smaller chemically-tagged cogwheels involving 4,4'-biphenyl spacers was tackled. In a similar way, it was envisioned to introduce first the distinct paddle *via* a chemoselective aryl-aryl bond formation starting from mono-iodinated key precursor **1**, and subsequently couple the four remaining bromophenylene moieties.

A huge variety of catalytic systems are known to achieve biaryl couplings, many of them involving palladium species.<sup>38</sup> Based on the higher reactivity of aryl iodides than that of aryl bromides in the oxidative addition elementary step, successful examples of chemoselective monocoupling of bromoiodobenzene derivatives have been reported, but the extent of the selectivity relies on a subtle interplay between the nature of the coupling partner (and thus the cross-coupling type), the choice of the pre-catalyst and ligand system, the steric and electronic bias of the substrate, and the reaction conditions. In addition, our star-shaped ruthenium-based system includes four bromophenyl and one single iodophenyl positions that are spatially and electronically decoupled, and thus they react fully independently. As mentioned earlier, they are highly deactivated by the central electron-rich cyclopentadienyl ring, and the choice of catalyst is restricted to highly active systems, which is not in favour of a Br *vs.* I discrimination. An extensive optimisation was not desirable at that stage of a multi-step synthesis, involving costly and structurally complex coupling partners. It was thus decided to carry on with Suzuki–Miyaura cross-couplings for the creation of the aryl–aryl bond, even though very few examples of successful iodo- *vs.* bromoaryl discrimination have been reported in unbiased substrates.<sup>43</sup> Interestingly, it has been inferred that substituting aryl bromide with aryl iodide leads to a change from oxidative addition to transmetalation in the rate-determining elementary step of such a cross-coupling.<sup>44</sup> Given the success encountered in Sonogashira monocoupling on the monoiodinated ruthenium complex, it appears that temperature-controlled selective

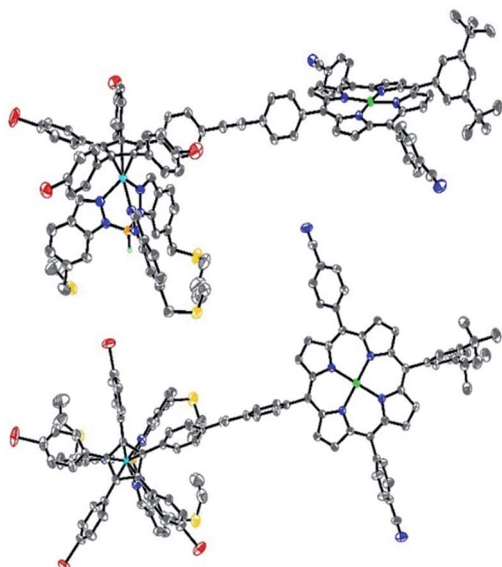
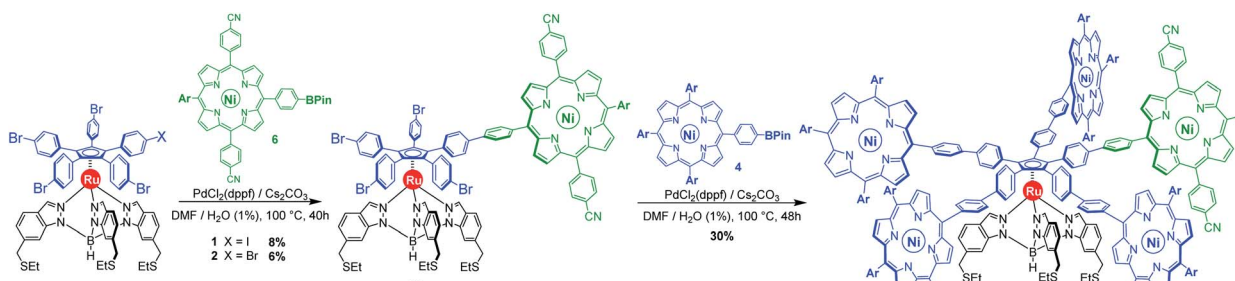


Fig. 5 Side view (top) and top view (bottom) of the molecular structure of monoporphyrinic ruthenium complex **13**. Thermal ellipsoids are drawn at 30% probability, and hydrogen atoms (except for B–H), solvent molecules and disordered atoms are omitted for clarity.



**Scheme 4** Synthesis of the chemically-tagged cogwheel **11**, incorporating one distinct electron-deficient porphyrinic macrocycle (in green), via sequential Suzuki–Miyaura cross-coupling reactions. Ar = 3,5-di-*tert*-butylphenyl.

oxidative addition of the iodophenyl fragment is possible in our system, and we thus intended to facilitate the transmetalation step while maintaining mild temperature conditions as a way to ensure chemoselectivity. Our attention was drawn by the copper-mediated Suzuki–Miyaura coupling conditions reported by Savarin and Liebeskind, exhibiting high efficiency with aryl iodides as substrates in a nonbasic medium at room temperature.<sup>45</sup> This palladium-catalysed process involves the copper(I) thiophene-2-carboxylate (CuTC) complex as a stoichiometric additive, which has been shown to facilitate the B to Pd transmetalation step when using arylboronic acids as coupling partners. Under such mild conditions, high I *vs.* Br selectivity has been reported on a simple bromoiodobenzene substrate, which prompted us to test these conditions on our more structurally complex system. A *trans* A<sub>2</sub>BC-type porphyrin carrying two electron-withdrawing 4-cyanophenyl substituents on the 10- and 20-positions as well as a phenylboronic acid moiety was thus required. Unfortunately, we failed to obtain this coupling partner, presumably due to nickel(II)-mediated homocoupling side reactions during the metalation step.

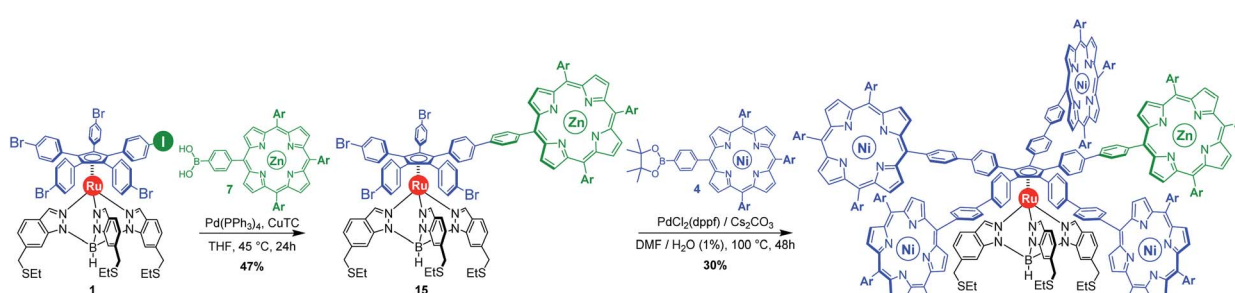
By default, a standard Suzuki–Miyaura cross-coupling was attempted, involving equimolar amounts of unsymmetrical moniodinated complex **1** and nickel(II) porphyrin **6** incorporating a boronic acid pinacol ester moiety (Scheme 4). In the presence of PdCl<sub>2</sub>(dpdpf) (10 mol%) as a catalyst and 2 equiv. of Cs<sub>2</sub>CO<sub>3</sub> as a base in a DMF/water (99 : 1) system, no conversion was observed at room temperature. Heating to 100 °C led to the formation of the desired monocoupled product, along with poly-substituted compounds. After tedious chromatographic

separation, the desired monoporphyrinic ruthenium complex **14** was finally isolated in 8% yield, which is comparable to the result of a statistical reaction on symmetrical pentabrominated complex **2** (6% yield). Such similar yields obtained with unsymmetrical and symmetrical penta(*p*-halogenophenyl) precursors **1** and **2** confirm that no significant chemoselectivity is achieved in our system with a Suzuki–Miyaura coupling solely catalysed by palladium. Moreover, formation of polyporphyrinic side products leads to a challenging purification, which explains the very low yields obtained in this step.

Subsequent four-fold biaryl coupling was carried out on monofunctionalised complex **14** with A<sub>3</sub>B-type porphyrin **4** as the coupling partner (8 equiv.) to afford in 30% yield the chemically-tagged cogwheel **11** possessing five shorter identical 4,4'-biphenyl linkers and distinct porphyrin paddles.

Two desymmetrised cogwheels of increasing diameter **11** and **10** were thus obtained *via* sequential reactions, with the first single coupling being either chemoselective or statistical. In these rotors, the contrast in STM images will stem from the electronic differentiation of one macrocyclic scaffold, bearing electron-withdrawing cyanophenyl substituents. As an alternative, it was also envisioned to change the nature of one metallic centre while keeping the macrocycle constant, and the corresponding cogwheel prototype involving one zinc(II) and four nickel(II) centres was next synthesised.

**2.3.3. A distinct metal as a chemical tag.** In anticipation of a possible copper-mediated Suzuki–Miyaura coupling for the monofunctionalisation step, the required zinc(II) porphyrin **7** (Fig. 3) carrying three 3,5-di-*tert*-butylphenyl substituents and



**Scheme 5** Synthesis of the chemically-tagged cogwheel **12**, incorporating one distinct zinc(II) porphyrin (in green), via sequential chemoselective Suzuki–Miyaura cross-coupling reactions. Ar = 3,5-di-*tert*-butylphenyl.

an additional phenylboronic acid moiety was prepared (see the ESI section†). The copper(i)-mediated single aryl–aryl coupling of monoiodinated key precursor **1** with boronic acid **7** (1.5 equiv.) was next attempted using  $\text{Pd}(\text{PPh}_3)_4$  (5 mol%) as the catalyst, in combination with CuTC (1.5 equiv.) in THF (Scheme 5). After 24 h at 45 °C, the desired monocoupled complex **15** incorporating a zinc(ii) porphyrinic unit and four remaining *p*-bromophenylene moieties was isolated in 47% yield. The efficiency of this single biaryl coupling appears comparable to that of the copper/palladium-cocatalysed Sonogashira mono-functionalisations performed previously on precursor **1** (Schemes 2 and 3), which reveals the high level of chemoselectivity achievable in copper-mediated Suzuki–Miyaura couplings under very mild conditions. It is noteworthy that an increase of the reaction temperature leads to complex mixtures of products, resulting from concurrent thermally-activated reactivity of the bromophenyl positions.

The monoporphyrinic ruthenium complex **15** was finally submitted to a four-fold Suzuki–Miyaura coupling under standard conditions with nickel(ii) porphyrin **4** bearing a phenylboronic acid pinacol ester substituent. The desired desymmetrised cogwheel **12** possessing four nickel(ii)  $\text{A}_3\text{B}$ -type porphyrins and a single zinc(ii) porphyrin, connected by five identical 4,4'-biphenyl linkers, was obtained in 30% yield. Thanks to Liebeskind copper-mediated conditions for the

selective monofunctionalisation of the pentahalogenated precursor, the overall yield for the synthesis of desymmetrised pentaporphyrinic cogwheels **11** and **12**, bearing 4,4'-biphenyl spacers, has undergone a six-fold increase and has now reached 3% over seven steps, starting from 3-amino-4-methylbenzoic acid.

Remarkably, the new cogwheel prototype **12** incorporates three distinct metal types shared on six different positions, with respective roles ranging from a mechanical ball bearing to electronic contrast agent.

#### 2.4. Spectroscopic and electrochemical studies of chemically-tagged cogwheels

The influence of the chemically-distinct porphyrinic paddle on the spectroscopic and electrochemical properties of the larger ethynyl-containing cogwheel **10** and smaller biphenylene-derived cogwheels **11** and **12** was investigated.

**2.4.1. NMR spectroscopy.** Our synthetic strategy involving the introduction of the distinct porphyrinic fragment in the first step allows a straightforward assignment of the signals in the  $^1\text{H}$  and  $^{13}\text{C}$  NMR spectra of the desymmetrised cogwheels **10**, **11** and **12**. These apparently complex spectra are highly similar to those of the corresponding symmetric cogwheels carrying five  $\text{A}_3\text{B}$ -type nickel(ii) porphyrins,<sup>35</sup> with the addition in an integration ratio of 1 : 4 of the signals of the chemically-tagged

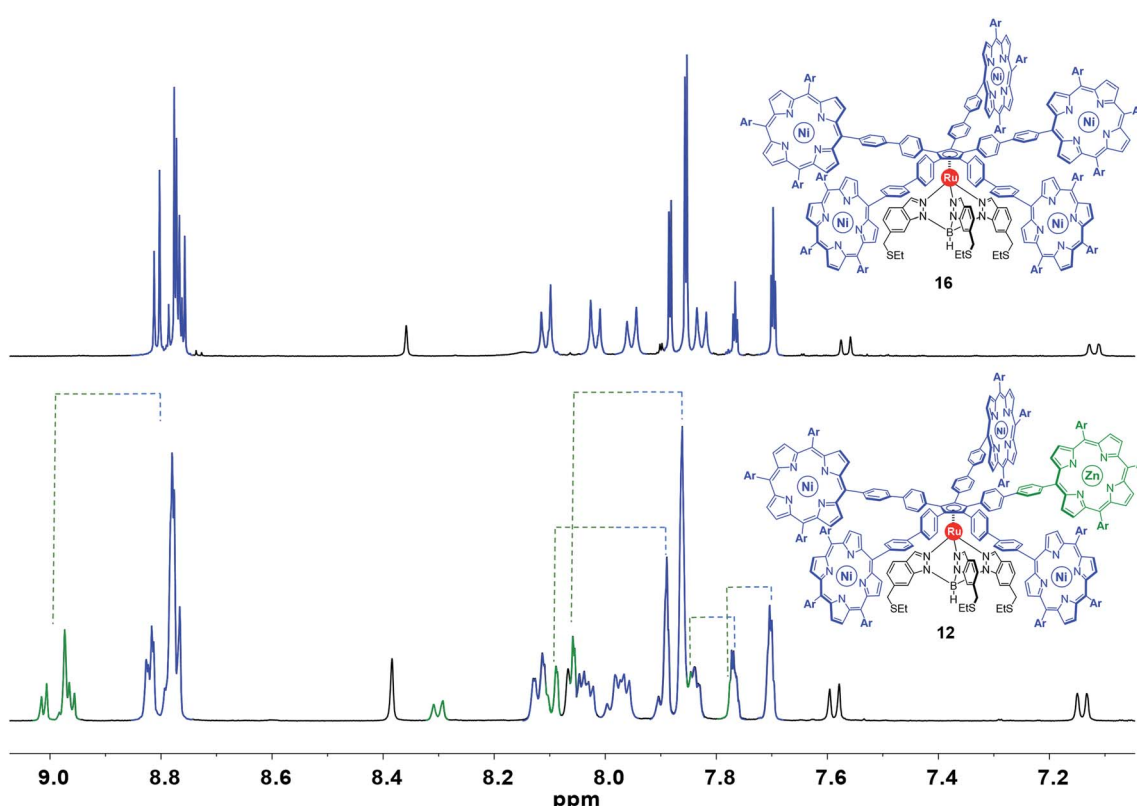


Fig. 6 Aromatic region of the  $^1\text{H}$  NMR spectrum (500 MHz,  $\text{CD}_2\text{Cl}_2$ ) of the symmetric cogwheel prototype **16** bearing 4,4'-biphenyl spacers and  $\text{A}_3\text{B}$ -type nickel(ii) 10,15,20-tris(3,5-di-tert-butylphenyl)porphyrins<sup>35</sup> (top) and of the desymmetrised cogwheel prototype **12** incorporating an  $\text{A}_3\text{B}$ -type zinc(ii) porphyrin as the chemical tag. Spectra are coloured in black, green and blue according to each fragment of the molecules ( $\text{Ar} = 3,5\text{-di-}t\text{-butylphenyl}$ ).



porphyrin (as identified in the spectra of intermediates **13**, **14** and **15**). This implies that the incorporation of a distinct porphyrin has a minor impact on the environment of the ruthenium-based cogwheel. In  $^1\text{H}$  and  $^{13}\text{C}$  NMR, the signals related to the tripodal ligand, the phenylethynylphenyl or 4,4'-biphenyl spacers and the four A<sub>3</sub>B-type nickel(II) porphyrins remain unchanged, as exemplified in Fig. 6 (signals depicted in blue and black) in the case of cogwheel **12**. In contrast, specific patterns for the distinct porphyrin (A<sub>2</sub>BC-type nickel(II) porphyrin for **10** and **11**, or A<sub>3</sub>B-type zinc(II) porphyrin for **12**) are observed, in particular for the  $\beta$ -pyrrole protons (8.5–9.0 ppm region) and for the aromatic protons of the 3,5-bis-*tert*-butylphenyl moiety. This has been highlighted in green in Fig. 6 in the case of compound **12**, for which the nature of the metal was expected to behave as a chemical tag. Indeed, all the signals belonging to the zinc(II) porphyrin and its *meso* substituents are clearly shifted downfield under the influence of the zinc centre, compared to the nickel(II) counterparts. This electron-deficient character of the zinc(II) porphyrinic fragment is very promising to generate spatial contrast in on-surface STM studies of single-molecules.

In addition, it is important to mention that porphyrins undergo unrestricted rotation around the phenylethynylphenyl or 4,4'-biphenyl axes, and that free rotation around the Cp–Ru–B axis takes place at room temperature. Variable-temperature  $^1\text{H}$  NMR experiments in  $\text{CD}_2\text{Cl}_2$  down to  $-60\text{ }^\circ\text{C}$  did not reveal any restricted rotation.

**2.4.2. UV/Vis absorption spectroscopy.** The UV/Vis spectra of desymmetrised pentaporphyrinic cogwheels **10**–**12** in dichloromethane are depicted in Fig. 7 (left). They all display an intense Soret band toward 418 nm and a weaker Q band around 529 nm, characteristic of nickel(II) porphyrins. A slight red shift of the Soret band is observed for cogwheel **12** (421 nm) along with the presence of extra Q bands around 548 and 586 nm, typical of zinc(II) porphyrins. Comparison of the Soret and Q bands of cogwheels **10** (black curve) and **11** (red curve), which only differ by the linkers around the cyclopentadienyl core, reveals that the molar extinction coefficient of the porphyrinic units depends on the nature of the spacer, with higher values (+14%) obtained for the shorter 4,4'-biphenyl pattern.

Additional absorption between 250 and 370 nm corresponds to the  $\pi$ – $\pi^*$  transition of the pentaarylcylopentadienyl core, with a clear influence of the nature of the linker leading to a bathochromic shift for the extended phenylethynylphenyl substituents (black curve).

In Fig. 7 (right), comparison of porphyrinic precursors **4** (dashed curve) and **7** (pink curve) highlights the known stronger absorption of zinc(II) porphyrins than that of nickel(II) analogues, which is further evidenced by the left spectrum with the zinc-containing cogwheel **12** having the highest molar extinction coefficient in the Soret band. Interestingly, sequential addition of porphyrin units on the ruthenium-based scaffold does not modify the absorption properties of each subunit, thus showing that the pentaarylcylopentadienyl ruthenium(II) centre and the porphyrins are electronically decoupled (Fig. 7, right). Moreover, the intensity of the Soret and Q bands in such porphyrinic complexes (e.g. **15** vs. **12**) is directly proportional to the number of porphyrins present in the molecular structure, thus revealing the additivity of chromophores' absorption properties in ruthenium complexes **10**–**12**.

**2.4.3. Electrochemistry.** The redox properties of the chemically-tagged cogwheels were examined by means of cyclic voltammetry performed in dichloromethane. The voltammogram of the oxidation region of pentaporphyrinic complex **10** is presented in Fig. 8 (black curve) and it exhibits four successive redox waves. The first two waves can be attributed to the one electron oxidation of the ruthenium(II) centre ( $E_{1/2} = 0.74\text{ V}$  vs. SCE) followed by the oxidation of the four A<sub>3</sub>B-type nickel(II) porphyrins ( $E_{1/2} = 0.95\text{ V}$  vs. SCE), by analogy with the symmetrical prototype reported previously.<sup>35</sup> The next two waves are related to successive one-electron oxidations of the distinct A<sub>2</sub>BC-type nickel(II) porphyrin carrying 4-cyanophenyl electron-withdrawing substituents ( $E_{1/2} = 1.13\text{ V}$  and  $1.30\text{ V}$  vs. SCE), in line with the oxidation potentials measured for the corresponding porphyrinic precursor **5** (see Fig. S4†). In contrast, as presented in Fig. 8 (purple curve), the first oxidation in chemically-tagged cogwheel **12** takes place on the distinct zinc(II) porphyrinic unit ( $E_{1/2} = 0.63\text{ V}$  vs. SCE) followed by the respective oxidations of the ruthenium centre ( $E_{1/2} = 0.74\text{ V}$  vs.

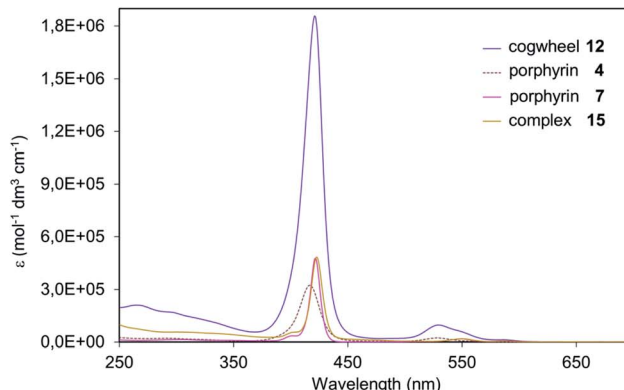
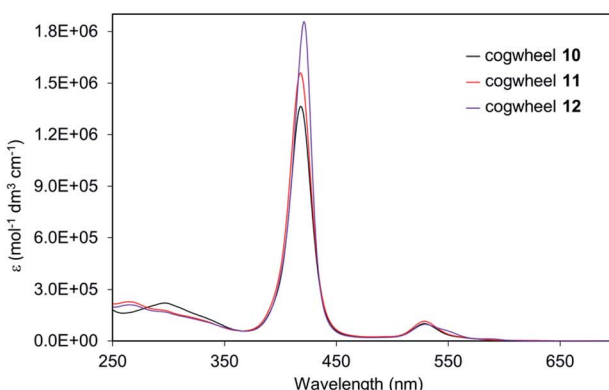


Fig. 7 UV/Vis absorption spectra of desymmetrised pentaporphyrinic cogwheels **10**, **11** and **12** (left) and of the series of compounds including porphyrins **4** and **7**, complex **15** and cogwheel **12** (right) in  $\text{CH}_2\text{Cl}_2$ .



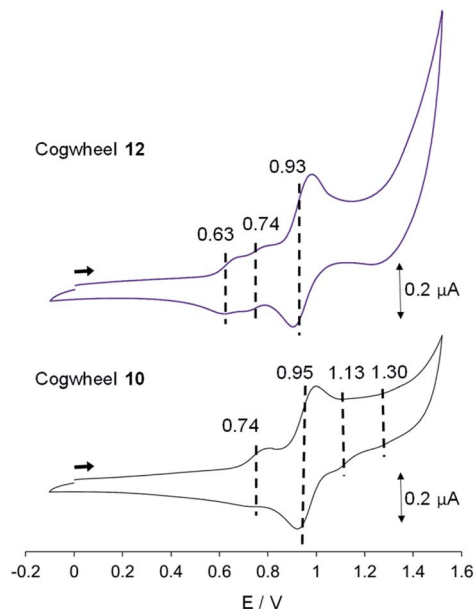


Fig. 8 Cyclic voltammograms of cogwheels **10** and **12** versus SCE ( $\text{CH}_2\text{Cl}_2$ ,  $0.1 \text{ M } n\text{Bu}_4\text{NPF}_6$ ,  $25^\circ\text{C}$ , scan rate:  $0.1 \text{ V s}^{-1}$ ).

SCE) and the four nickel(II) A<sub>3</sub>B-type porphyrins ( $E_{1/2} = 0.93 \text{ V vs. SCE}$ ).

In the reduction region of the voltammogram (Fig. S4 and S5 in the ESI section†), no reversible wave is observed for ruthenium-based cogwheels **10** and **12** down to the voltage limit of  $-1.5 \text{ V}$ . However, the first reduction of the porphyrin precursor **5** carrying two 4-cyanophenyl substituents occurs reversibly at  $E_{1/2} = -1.25 \text{ V}$  (vs. SCE) and this redox behaviour is still observed in the corresponding monoporphyrinic ruthenium complex **13**. It can thus be inferred that the first reduction in pentaporphyrinic complex **10** will take place on the tagged A<sub>2</sub>BC nickel(II) porphyrin, in line with its electron-deficient character compared to the remaining A<sub>3</sub>B nickel(II) porphyrins. This localised redox behaviour will be exploited in on-surface STM studies to induce contrast within the single molecular cogwheel.

### 3. Conclusion

Four desymmetrised pentaporphyrinic molecular gears were carefully designed and synthesised, with the aim of assembling them into trains of gears on a surface and ultimately achieving controlled intermolecular gearing. These star-shaped organometallic structures incorporate a hydrotris(indazolyl)borate ligand as an anchor to prevent diffusion on the surface, a central ruthenium atom as a fixed rotation axis, and an azimuthal pentaporphyrinic cyclopentadienyl cogwheel specifically labelled for STM studies.

Desymmetrisation of the cogwheel architecture was first achieved by introducing one tooth longer than the other four, using a phenylethynylphenyl spacer instead of a 4,4'-biphenylene between the porphyrinic macrocycle and the cyclopentadienyl core. To allow for optimal mechanical interactions

within the trains of gears, chemical labelling was next investigated as a way to induce local submolecular contrast in STM images while maintaining identical lengths and homogeneous peripheral shapes for the paddles. The electronic properties of one single porphyrinic paddle were successfully modulated either by introducing electron-withdrawing *p*-cyanophenyl substituents on the tetrapyrrole core or by changing the nature of the central metal from nickel(II) to zinc(II), as evidenced by spectroscopic and electrochemical studies.

To reach the required structural diversity, a modular synthetic approach was followed, relying on a penta(*p*-halogenophenyl)cyclopentadienyl ruthenium(II) key building block, bearing a single pre-activated *p*-iodophenyl group. Post-functionalisation was achieved *via* sequential palladium-catalysed cross-coupling reactions, starting with a chemoselective coupling of the iodophenylene moiety under Sonogashira or more challenging Suzuki–Miyaura conditions, requiring the assistance of copper(I) additives. This controlled introduction of the sterically- or chemically-tagged porphyrinic tooth followed by four-fold cross-couplings on the remaining *p*-bromophenyl positions yielded four prototypes of desymmetrised pentaporphyrinic molecular gears with diameters over 5 nm. Mechanical studies on surfaces and on the single molecule scale are currently underway.

### Conflicts of interest

There are no conflicts to declare.

### Acknowledgements

This work was supported by Paul Sabatier University (Toulouse) and CNRS. It has received funding from the ANR (ACTION project ANR-15-CE29-0005), the European Union's Horizon 2020 research and innovation programme under the project MEMO, grant agreement no. 766864, the JSPS KAKENHI grant in aid for Scientific Research on Innovative Areas "Molecular Engine (no. 8006)" 18H05419 and the KAKENHI Grant-in-Aid for Challenging Research (20K21131). DFT calculations were performed using HPC resources from CALMIP (grant 2020-p20041). Y. G. thanks the French Ministry of National Education for a PhD Fellowship. Dr Jacques Bonvoisin is gratefully acknowledged for his help with cyclic voltammetry experiments.

### Notes and references

- (a) J.-P. Sauvage, *Angew. Chem., Int. Ed.*, 2017, **56**, 11080–11093; (b) J. F. Stoddart, *Angew. Chem., Int. Ed.*, 2017, **56**, 11094–11125; (c) B. L. Feringa, *Angew. Chem., Int. Ed.*, 2017, **56**, 11060–11078.
- (a) V. Balzani, A. Credi and M. Venturi, *Molecular Devices and Machines. Concepts and Perspectives for the Nanoworld*, Wiley-VCH, Weinheim, 2nd edn, 2008; (b) S. Erbas-Cakmak, D. A. Leigh, C. T. McTernan and A. L. Nussbaumer, *Chem. Rev.*, 2015, **115**, 10081–10206.
- (a) G. Rapenne, *Org. Biomol. Chem.*, 2005, **3**, 1165–1169; (b) A. A. Gakh, *Molecular Devices: An Introduction to*



*Technomimetics and Its Biological Applications*, John Wiley & Sons, Hoboken, NJ, 2018; (c) C. Kammerer, G. Erbland, Y. Gisbert, T. Nishino, K. Yasuhara and G. Rapenue, *Chem. Lett.*, 2019, **48**, 299–308.

4 A. Ikeda, T. Tsudera and S. Shinkai, *J. Org. Chem.*, 1997, **62**, 3568–3574.

5 G. Rapenue and G. Jimenez-Bueno, *Tetrahedron*, 2007, **63**, 7018–7026.

6 (a) Y. Shirai, A. J. Osgood, Y. Zhao, K. F. Kelly and J. M. Tour, *Nano Lett.*, 2005, **5**, 2330–2334; (b) T. Kudernac, N. Ruangsrapichat, M. Parschau, B. Maciá, N. Katsonis, S. R. Harutyunyan, K.-H. Ernst and B. L. Feringa, *Nature*, 2011, **479**, 208–211; (c) T. Nishino, C. J. Martin, H. Takeuchi, F. Lim, K. Yasuhara, Y. Gisbert, S. Abid, N. Saffon-Merceron, C. Kammerer and G. Rapenue, *Chem.-Eur. J.*, 2020, **26**, 12010–12018.

7 T. Muraoka, K. Kinbara, Y. Kobayashi and T. Aida, *J. Am. Chem. Soc.*, 2003, **125**, 5612–5613.

8 J. D. Badjic, V. Balzani, A. Credi, S. Silvi and J. F. Stoddart, *Science*, 2004, **303**, 1845–1849.

9 (a) S. Kassem, T. van Leeuwen, A. S. Lubbe, M. R. Wilson, B. L. Feringa and D. A. Leigh, *Chem. Soc. Rev.*, 2017, **46**, 2592–2621; (b) M. Baroncini, S. Silvi and A. Credi, *Chem. Rev.*, 2020, **120**, 200–268; (c) D. Dattler, G. Fuks, J. Heiser, E. Moulin, A. Perrot, X. Yao and N. Giuseppone, *Chem. Rev.*, 2020, **120**, 310–433; (d) V. García-López, D. Liu and J. M. Tour, *Chem. Rev.*, 2020, **120**, 79–124; (e) A. Goswami, S. Saha, P. K. Biswas and M. Schmittel, *Chem. Rev.*, 2020, **120**, 125–199.

10 T. R. Kelly, H. De Silva and R. A. Silva, *Nature*, 1999, **401**, 150–152.

11 N. Koumura, R. W. J. Zijlstra, R. A. van Delden, N. Harada and B. L. Feringa, *Nature*, 1999, **401**, 152–155.

12 (a) H. L. Tierney, C. J. Murphy, A. D. Jewell, A. E. Baber, E. V. Iski, H. Y. Khodaverdian, A. F. McGuire, N. Klebanov and E. C. H. Sykes, *Nat. Nanotechnol.*, 2011, **6**, 625–629; (b) U. G. E. Perera, F. Ample, H. Kersell, Y. Zhang, G. Vives, J. Echeverria, M. Grisolia, G. Rapenue, C. Joachim and S.-W. Hla, *Nat. Nanotechnol.*, 2013, **8**, 46–51.

13 (a) L. Grill, K.-H. Rieder, F. Moresco, G. Rapenue, S. Stojkovic, X. Bouju and C. Joachim, *Nat. Nanotechnol.*, 2007, **2**, 95–98; (b) W.-H. Soe, Y. Shirai, C. Durand, Y. Yonamine, K. Minami, X. Bouju, M. Kolmer, K. Ariga, C. Joachim and W. Nakanishi, *ACS Nano*, 2017, **11**, 10357–10365; (c) W.-H. Soe, C. Durand, O. Guillermet, S. Gauthier, H.-P. Jacquot de Rouville, S. Srivastava, C. Kammerer, G. Rapenue and C. Joachim, *Nanotechnology*, 2018, **29**, 495401; (d) F. Eisenhut, J. Meyer, J. Krüger, R. Ohmann, G. Cuniberti and F. Moresco, *Surf. Sci.*, 2018, **678**, 177–182; (e) Y. Zhang, J. P. Calupitan, T. Rojas, R. Tumbleson, G. Erbland, C. Kammerer, T. M. Ajayi, S.-W. Wang, L. A. Curtiss, A. T. Ngo, S. E. Ulloa, G. Rapenue and S.-W. Hla, *Nat. Commun.*, 2019, **10**, 3742; (f) G. J. Simpson, V. García-López, A. D. Boese, J. M. Tour and L. Grill, *Nat. Commun.*, 2019, **10**, 4631.

14 C. Joachim and G. Rapenue, *ACS Nano*, 2013, **7**, 11–14.

15 G. Rapenue and C. Joachim, *Nat. Rev. Mater.*, 2017, **2**, 17040–17042.

16 T. Freeth, A. Jones, J. M. Steele and Y. Bitsakis, *Nature*, 2008, **454**, 614–617.

17 J. Yang, J. Deng, C. Troadec, T. Ondarçuhu and C. Joachim, *Nanotechnology*, 2014, **25**, 465305.

18 W. D. Hounshell, C. A. Johnson, A. Guenzi, F. Cozzi and K. Mislow, *Proc. Natl. Acad. Sci. U. S. A.*, 1980, **77**, 6961–6964.

19 Y. Kawada and H. Iwamura, *J. Org. Chem.*, 1980, **45**, 2547–2548.

20 H. Iwamura, T. Ito, H. Ito, K. Toriumi, Y. Kawada, E. Osawa, T. Fujiyoshi and C. Jaime, *J. Am. Chem. Soc.*, 1984, **106**, 4712–4717.

21 D. K. Frantz, A. Linden, K. K. Baldridge and J. S. Siegel, *J. Am. Chem. Soc.*, 2012, **134**, 1528–1535.

22 K. H. Au Yeung, T. Kühne, F. Eisenhut, M. Kleinwächter, Y. Gisbert, R. Robles, N. Lorente, G. Cuniberti, C. Joachim, G. Rapenue, C. Kammerer and F. Moresco, *J. Phys. Chem. Lett.*, 2020, **11**, 6892–6899.

23 W.-H. Soe, S. Srivastava and C. Joachim, *J. Phys. Chem. Lett.*, 2019, **10**, 6462–6467.

24 (a) H. Iwamura and K. Mislow, *Acc. Chem. Res.*, 1988, **21**, 175–182; (b) K. Okamura, Y. Inagaki, H. Momma, E. Kwon and W. Setaka, *J. Org. Chem.*, 2019, **84**, 14636–14643.

25 W. Setaka, T. Nirengi, C. Kabuto and M. Kira, *J. Am. Chem. Soc.*, 2008, **130**, 15762–15763.

26 H. Ube, Y. Yasuda, H. Sato and M. Shionoya, *Nat. Commun.*, 2017, **8**, 14296.

27 (a) F. Huang, G. Wang, L. Ma, Y. Wang, X. Chen, Y. Che and H. Jiang, *J. Org. Chem.*, 2017, **82**, 12106–12111; (b) X. Jiang, S. Yang, M. J. Jellen, K. N. Houk and M. Garcia-Garibay, *Org. Lett.*, 2020, **22**, 4049–4052.

28 (a) A. M. Stevens and C. J. Richards, *Tetrahedron Lett.*, 1997, **38**, 7805–7808; (b) S. Ogi, T. Ikeda, R. Wakabayashi, S. Shinkai and M. Takeuchi, *Chem.-Eur. J.*, 2010, **16**, 8285–8290.

29 (a) M. Nakamura, K. Kishimoto, Y. Kobori, T. Abe, K. Yoza and K. Kobayashi, *J. Am. Chem. Soc.*, 2016, **138**, 12564–12577; (b) H. Ube, R. Yamada, J. Ishida, H. Sato, M. Shiro and M. Shionoya, *J. Am. Chem. Soc.*, 2017, **139**, 16470–16473; (c) S. Toyota, K. Kawahata, K. Sugahara, T. Oki and T. Iwanaga, *Asian J. Org. Chem.*, 2019, **8**, 1919–1923.

30 (a) N. Tanaka, Y. Inagaki, K. Yamaguchi and W. Setaka, *Cryst. Growth Des.*, 2020, **20**, 1097–1102; (b) I. Liepuoniute, M. J. Jellen and M. A. Garcia-Garibay, *Chem. Sci.*, 2020, **11**, 12994–13007.

31 (a) F. Chiaravalloti, L. Gross, K.-H. Rieder, S. M. Stojkovic, A. Gourdon, C. Joachim and F. Moresco, *Nat. Mater.*, 2007, **6**, 30–33; (b) C. Manzano, W.-H. Soe, H. S. Wong, F. Ample, A. Gourdon, N. Chandrasekhar and C. Joachim, *Nat. Mater.*, 2009, **8**, 576–579.

32 W.-H. Soe, M. Kleinwächter, C. Kammerer, G. Rapenue and C. Joachim, *J. Phys. Chem. C*, 2020, **124**, 22625–22630.

33 G. Vives, H.-P. Jacquot de Rouville, A. Carella, J.-P. Launay and G. Rapenue, *Chem. Soc. Rev.*, 2009, **38**, 1551–1561.

34 C. Kammerer and G. Rapenue, *Eur. J. Inorg. Chem.*, 2016, 2214–2226.



35 G. Erbland, S. Abid, Y. Gisbert, N. Saffon-Merceron, Y. Hashimoto, L. Andreoni, T. Guérin, C. Kammerer and G. Rapenne, *Chem.-Eur. J.*, 2019, **25**, 16328–16339.

36 G. Erbland, Y. Gisbert, G. Rapenne and C. Kammerer, *Eur. J. Org. Chem.*, 2018, 4731–4739.

37 R. Chinchilla and C. Nájera, *Chem. Soc. Rev.*, 2011, **40**, 5084–5121.

38 J. Hassan, M. Sévignon, C. Gozzi, E. Schulz and M. Lemaire, *Chem. Rev.*, 2002, **102**, 1359–1470.

39 Y. Gisbert, S. Abid, G. Bertrand, N. Saffon-Merceron, C. Kammerer and G. Rapenne, *Chem. Commun.*, 2019, **55**, 14689–14692.

40 Y. Zhang, H. Kersell, R. Stefak, J. Echeverria, V. Iancu, U. G. E. Perera, Y. Li, A. Deshpande, K.-F. Braun, C. Joachim, G. Rapenne and S.-W. Hla, *Nat. Nanotechnol.*, 2016, **11**, 706–712.

41 (a) M. J. Frisch, *et al.*, *Gaussian 09 Revision D.01*, Gaussian Inc., Wallingford CT, 2013, (see ESI† for full author list); (b) C. Bannwarth, S. Ehlert and S. Grimme, *J. Chem. Theory Comput.*, 2019, **15**, 1652–1671.

42 H. Marbach, *Acc. Chem. Res.*, 2015, **48**, 2649–2658.

43 Stille cross-couplings have been far more documented for aryl bromide vs. aryl iodide discrimination but preliminary studies involving monoiodinated key precursor **1** and a tributyl(*p*-tolyl)stannane as a model coupling partner failed to give the desired monocoupled product in satisfactory yield.

44 (a) G. B. Smith, G. C. Dezeny, D. L. Hughes, A. O. King and T. R. Verhoeven, *J. Org. Chem.*, 1994, **59**, 8151–8156; (b) A. F. Littke, C. Dai and G. C. Fu, *J. Am. Chem. Soc.*, 2000, **122**, 4020–4028.

45 C. Savarin and L. S. Liebeskind, *Org. Lett.*, 2001, **3**, 2149–2152.

